

# Intravoxel Incoherent Motion (IVIM)\* *f*-maps of Pancreatic Lesions

Re, Thomas Joseph, M.D., MSEE<sup>1</sup>; Klauss, Miriam, M.D.<sup>2</sup>; Lemke, Andreas, MSc<sup>3,4</sup>; Laun, Frederik, Ph.D.<sup>4</sup>; Simon, Dirk, MSc<sup>1</sup>; Delorme, Stefan, M.D.<sup>1</sup>; Stieltjes, Bram, M.D.<sup>1</sup>

<sup>1</sup>German Cancer Research Center (DKFZ), Department of Radiology – E 010, Heidelberg, Germany

<sup>2</sup>Department of Diagnostic Radiology, University of Heidelberg, Heidelberg, Germany

<sup>3</sup>Department of Computer Assisted Clinical Medicine, University of Heidelberg, Mannheim, Faculty of Medicine, Mannheim, Germany

<sup>4</sup>German Cancer Research Center (DKFZ), Department of Physics in Radiology – E 020, Heidelberg, Germany

## Abstract

**Purpose:** To illustrate our experience using diffusion-weighted (DW) derived IVIM perfusion fraction *f* images (*f*-maps) for the delineation of solid pancreatic lesions. Particular attention is given to the comparison of this experimental technique with the clinically established technique of ADC-mapping.

**Methods:** Seven representative cases (1 healthy volunteer, 4 pancreatic adenocarcinoma cases, and 2 pancreatitis cases) are presented. Each were examined with contrast-enhanced T1 and T2-weighted magnetic resonance (MR) and with echo-planar MR diffusion-weighted imaging (DWI) using eleven different b-values ranging from 0–800 s/mm<sup>2</sup>. The DWI data was fitted to both the “Incoherent Intra-Voxel Motion” (IVIM) model and a linear apparent diffusion constant (ADC) equation, and the perfusion fraction *f* and ADC-maps were calculated. As a novel approach, ADC and *f*-map data was combined to identify vascular (high perfusion but low ADC) or bile duct (low perfusion but high ADC) voxels which were then color tagged on the *f*-map images.

**Results / Conclusion:** When compared to ADC-maps, *f*-maps improved the distinction between lesion and vessels, while ADC-maps more accurately identified adjacent pancreatic ducts. Images which integrate *f* and ADC data provided better lesion delineation than could be

achieved with either technique alone. Since *f*-maps do not require ionizing radiation nor contrast agent, they could be considered an alternative to CT and contrast-enhanced MRI techniques in patients with specific contraindications as well as in screening and follow-up imaging programs.

## Introduction

Contrast-enhanced magnetic resonance (MR) and computed tomography (CT) imaging are currently the standard imaging modalities for pancreatic lesions [1–3]. Their high diagnostic value unconsidered, they require intravenous contrast agent and, in the case of CT, ionizing radiation. Diffusion-weighted imaging (DWI) could prove a non-invasive alternative, since recent advances in scanner technologies, fast pulse sequences and parallel imaging have permitted its use in the abdomen where organ motion and tissue inhomogeneity have long prevented robust diffusion measurements [4–6]. Reports have shown that the DWI-derived apparent diffusion constant (ADC) can be used to monitor the pancreatic exocrine function in chronic pancreatitis [7, 8], for characterizing cystic lesions of the pancreas [9], and for detecting pancreatic cancer, which has a significantly lower ADC value than normal pancreas tissue [10–12].

Recently there has been growing interest in extracting perfusion information from diffusion-weighted data based on

the intravoxel incoherent motion (IVIM) model [13–15] first presented by LeBihan in 1986 [16, 17]. In this model, the diffusion-weighted signal is considered to be effected by two distinct types of molecular motion: *diffusion*, due to thermal Brownian motion, and *perfusion*, due to the microcirculation in capillaries. The IVIM model is represented mathematically by the equation:

$$\frac{S}{S_0} = (1-f) e^{-bD} + f e^{-b(D+D^*)}$$

where  $S/S_0$  is the signal decay measured in each individual voxel in the diffusion-weighted image, the b-value represents the strength of the diffusion weighting, D is the diffusion constant, D\* is the pseudo diffusion coefficient, and *f* is the perfusion fraction. This equation is a biexponential with the first term representing the pure diffusion influence on the diffusion-weighted signal, while the second term represents the pure perfusion influence on the diffusion-weighted signal. The perfusion fraction (*f*) indicates the relative influence of the second perfusion term and thus is correlated to the perfusion or microcirculation in the capillaries of the tissue under study. In a recent work, *f* was shown to be significantly lower within pancreatic tumors than in healthy pancreatic tissue [18]. Another study showed similar results for chronic pancreatitis mass formations [19]. Furthermore, *f* was shown to be

quantitatively superior to both ADC and D for characterizing pancreatic lesions [18]. Images created by mapping the *f* parameter as a gray scale (*f*-maps), hold important clinical information for both diagnosing and differentiating pancreatic lesions, but so far the reading of *f*-maps is unfamiliar to general radiologists. Thus, this pictorial essay aims to familiarize the clinician with this emerging imaging method. This work was generated within a cooperative project of Siemens Healthcare and the German national cancer center, diagnostic imaging for radio-oncology.

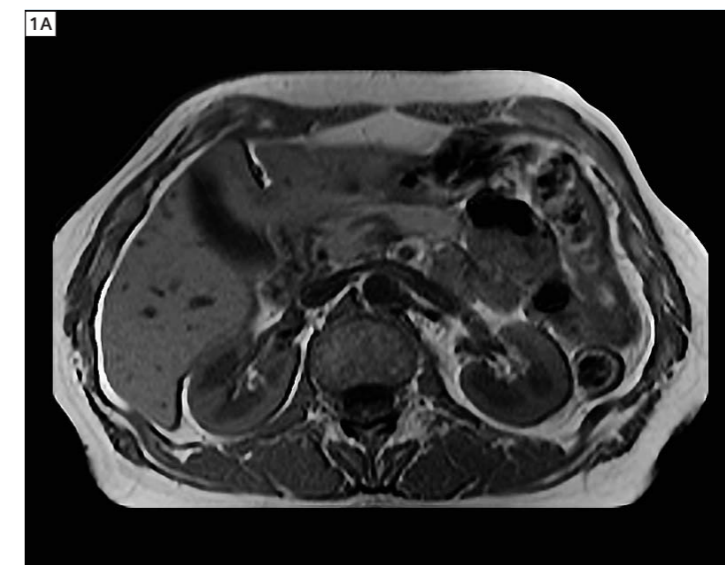
## Materials and methods

### Study population

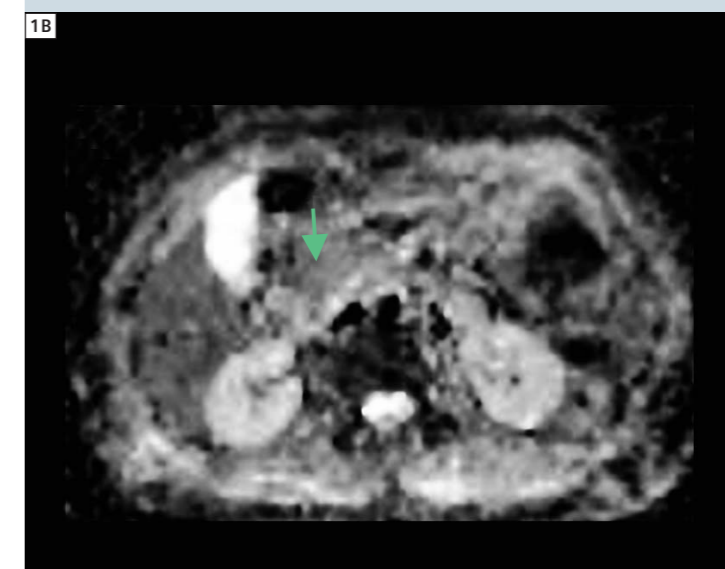
This work was generated within a cooperative project of Siemens Healthcare and the German national cancer center, diagnostic imaging for radio-oncology. The study protocol was approved by the Institutional Review Board. Informed consent was obtained from all subjects prior to the examination. In 2008 (June–December), 3 healthy volunteers, 14 patients with histopathologically proven pancreatic carcinoma (11 men and 3 women, age range 43–82, mean age 62.6) and 8 histopathologically verified pancreatitis patients (7 men and 1 woman, age range 40–74, mean age 55.5) were included consecutively during this period.

### MR examination

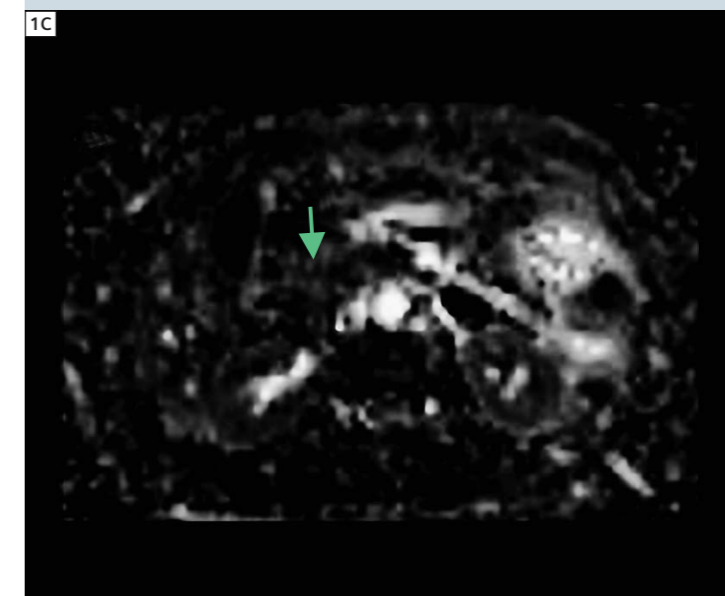
MR imaging was performed using a 1.5T scanner (MAGNETOM Avanto, Siemens Healthcare, Erlangen, Germany) with a maximum gradient strength of 45 mT/m using a six-element body-phased array coil and a 24-channel spine array coil. The routine pancreatic MR imaging protocol for the patient group consisted of TrueFISP imaging sequences (sagittal, axial and coronal) (TR/TE = 437.2/1.16 ms), breathhold (in expiration) dual gradient echo (2D) T1-weighted (T1w) imaging in transversal orientation (TR/TE = 110/4.82 ms), breathhold (expiration) single-shot turbo spin-echo T2-weighted (T2w) imaging in transversal and coronal orientation (TR/TE = 250/20 ms) and MR cholangiopancreatography in breathhold (expiration) single-shot turbo spin-echo (TR/TE = 4500/789 ms).



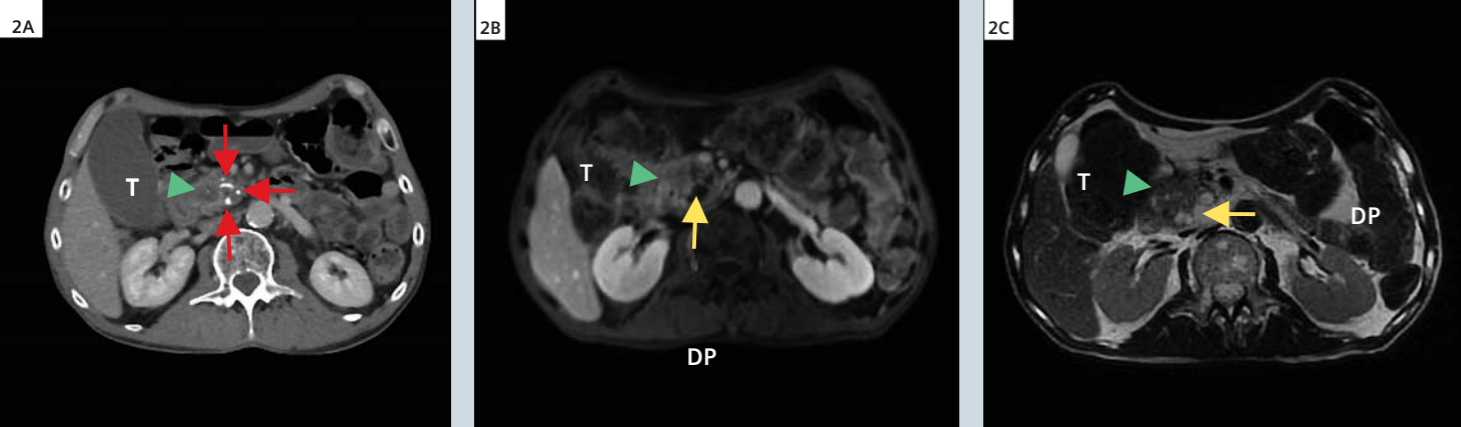
**1** Axial T1-weighted image of a healthy volunteer.



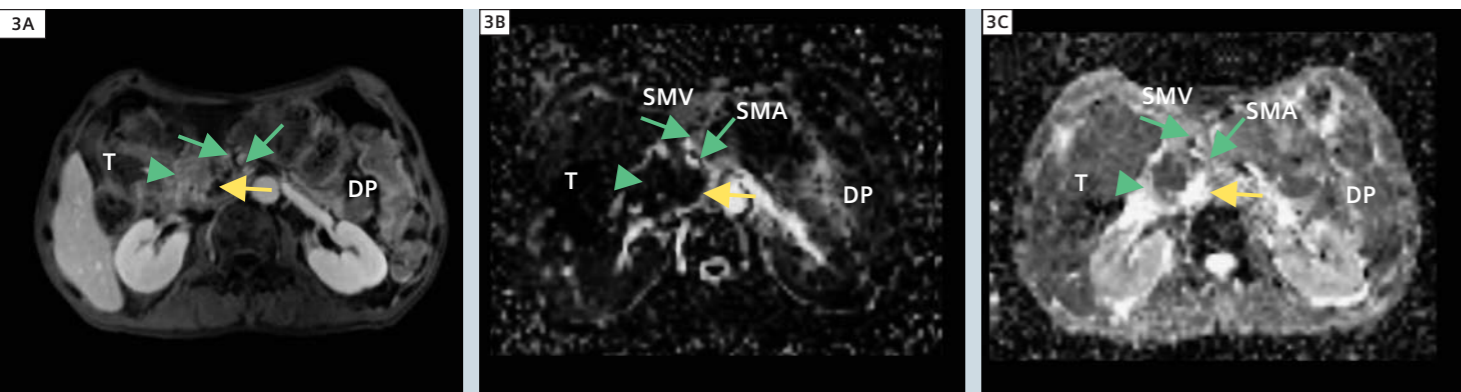
**1** In the ADC-map it can be seen that the pancreas (green arrow) appears iso-intense to the liver.



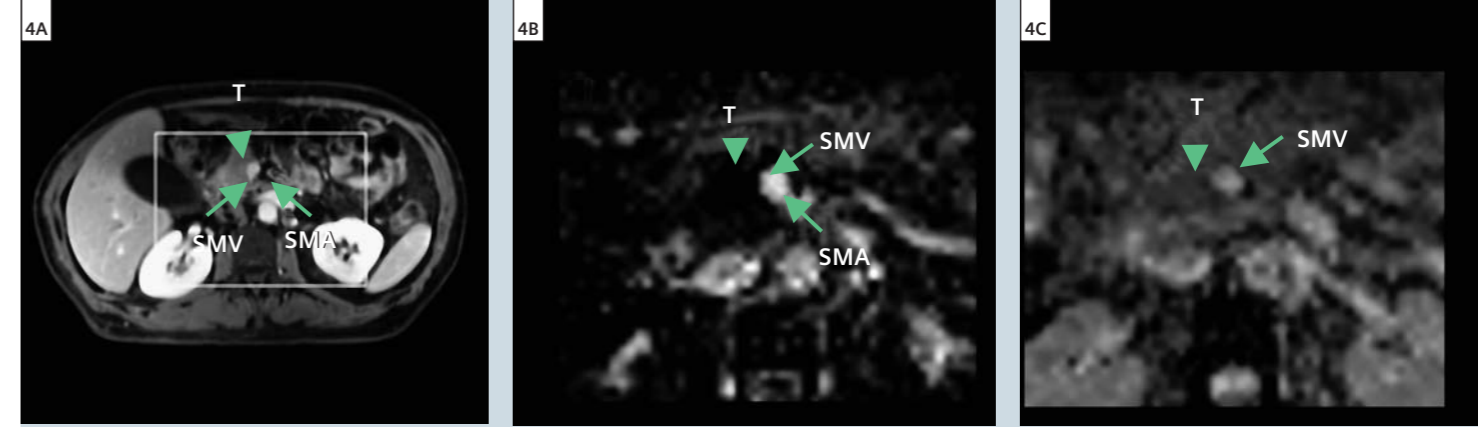
**1** In the *f*-map, the pancreas (green arrow) shows a mixed hypo- and hyper-intense signal.



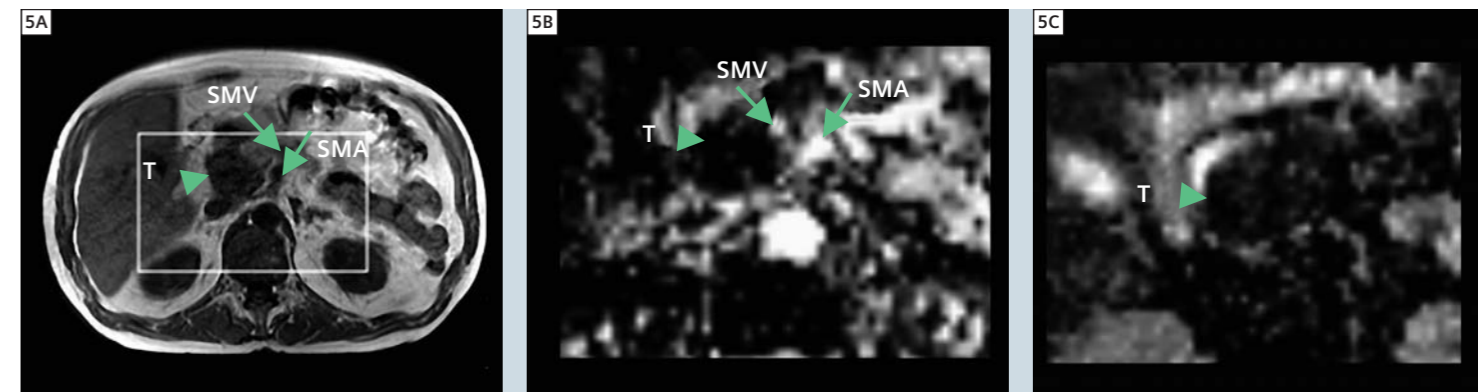
**2** Axial contrast-enhanced CT (A), contrast-enhanced T1w image (B) and T2w image (C) for a patient with chronic pancreatitis with calcifications (red arrows) within the pancreatic head (see CT on the left) as well as pancreatic cancer (green arrowhead). The dilated pancreatic duct can also be appreciated (yellow arrows). (T = tumor; DP = ductus pancreaticus).



**3** Axial T1w image (A), *f*-map (B) and ADC map (C) in the same patient with pancreatic cancer as shown in figure 2. The carcinoma can be seen as a hypointense area in both the *f* and the ADC-map (green arrowhead). Note that the hypointense area in the *f*-map is larger than that in the ADC-map because in the *f*-map the dilated pancreatic duct (long arrows) adjacent to the tumor is as hypointense as the tumor itself. Also appreciated in these images are the superior mesenteric artery (SMA) and superior mesenteric vein (SMV) (green arrows), which both appear bright in the *f*-map and in the T1w image. In the ADC-map, the SMV is visible but the SMA is not. The tumor is more easily evidenced in the *f*-map than in the conventional imaging. (T = tumor; DP = ductus pancreaticus (yellow arrow); SMA = superior mesenteric artery; SMV = superior mesenteric vein).



**4** Patient with pancreatic cancer tumor in the head of the pancreas (green arrowhead). The tumor is better delineated in the *f*-map (B) than in the ADC-map (C). Contact with the adjacent superior mesenteric vein (SMV) can be seen in all three images. Note that the superior mesenteric artery (SMA) is visible in the *f*-map but not in the ADC-map. T1w image (A) also provided for comparison. (white rectangle in T1w image = region displayed in other images; T = tumor; SMA = superior mesenteric artery; SMV = superior mesenteric vein).



**5** Axial T1w image (A), *f*-map (B) and ADC-map (C) in a patient with pancreatic cancer in the head of the pancreas (green arrowhead). The tumor margins are better seen in the *f*-map than in the ADC-map. Furthermore, the superior mesenteric artery (SMA) and vein (SMV) can be seen in the *f*-map (green arrows) but not in the ADC-map. (White rectangle in T1w image = region displayed in other images; T = tumor; SMA = superior mesenteric artery; SMV = superior mesenteric vein).

DWI was performed in addition to the routine MR imaging protocol. Diffusion-weighted images were acquired using a single-shot echo-planar imaging (SE-EPI) pulse sequence in end expiration breath-hold with the following imaging parameters: TR = 1300 ms, TE = 60 ms, FOV = 350 × 273 mm<sup>2</sup>, matrix size = 100 × 78, 14 slices, slice thickness/gap = 5/0.25 mm, 4 averages, bandwidth = 3000 Hz/Px, k-space based parallel imaging technique (*syngo* GRAPPA; Siemens Healthcare) used with an acceleration factor of two, b-values = 0, 25, 50, 75, 100, 150, 200, 300, 400, 600 and 800 s/mm<sup>2</sup> and a total measurement time of twelve minutes. The diffusion weighting was accomplished with a twice-refocused spin echo (TRSE) diffusion preparation and three orthogonal gradient directions (1,1,-1/2), (1,-1/2,1) and (-1/2,1,1) to

obtain trace-weighted images. The acquisition was separated into blocks (b<sub>0</sub>, b<sub>25</sub>), (b<sub>0</sub>, b<sub>50</sub>)... (b<sub>0</sub>, b<sub>800</sub>) and each block was acquired in a single breathhold (TA = 26 s) to avoid motion artifacts.

#### CT examination

Computed tomography (CT) scans of the patients were obtained from referring institutions.

#### Post processing and data analysis

DW-images were post-processed using software developed in-house based on the open source imaging software ImageJ (<http://rsb.info.nih.gov/ij>) applying two approaches:

- biexponential Levenberg-Marquardt based fitting to the IVIM-model equation (1) (see above) separating the contribution of microperfusion and

real diffusion in a DWI measurement. In this fit, the perfusion fraction *f* and the diffusion coefficient *D* were taken as free parameters, whereas the pseudo Diffusion Coefficient *D*<sup>\*</sup> was fixed at 20 μm<sup>2</sup>/ms.

- monoexponential linear least squares fitting to equation (2):

$$\ln \frac{S}{S_0} = -b(ADC)$$

using the total set of b-values yielding the Apparent Diffusion Coefficient ADC. The *f* parameter obtained through the first approach and the ADC parameter obtained through the second approach were mapped as a gray scale to create multi-slice *f*-map and ADC-maps. For two specific cases, the *f* and ADC data were combined to identify vascular

and bile duct voxels. Voxels with high perfusion (*f* > 0.35) but low ADC (ADC between 0.81 and 2.1 μm<sup>2</sup>/ms) were classified as vascular while those with low perfusion (*f* < 0.15) but high ADC (ADC between 1.5 and 2.5 μm<sup>2</sup>/ms) were classified as ductal. A color overlay was then used to depict vascular (red) and bile duct (blue) voxels on the *f*-maps. Images and parameter maps were read by two experienced radiologists in consensus. Pancreatic lesions were first identified in the routine CT and MR images. The lesions were then visually identified in the corresponding ADC and *f*-maps.

## Results

### Healthy volunteer

An example of normal ADC and *f*-map findings, taken from one of the healthy

volunteers is provided in figure 1. It can be seen that the pancreas (arrow) appears isointense to the liver in the ADC-map. In the *f*-map, the pancreas shows a mixed hypo- and hyperintense signal.

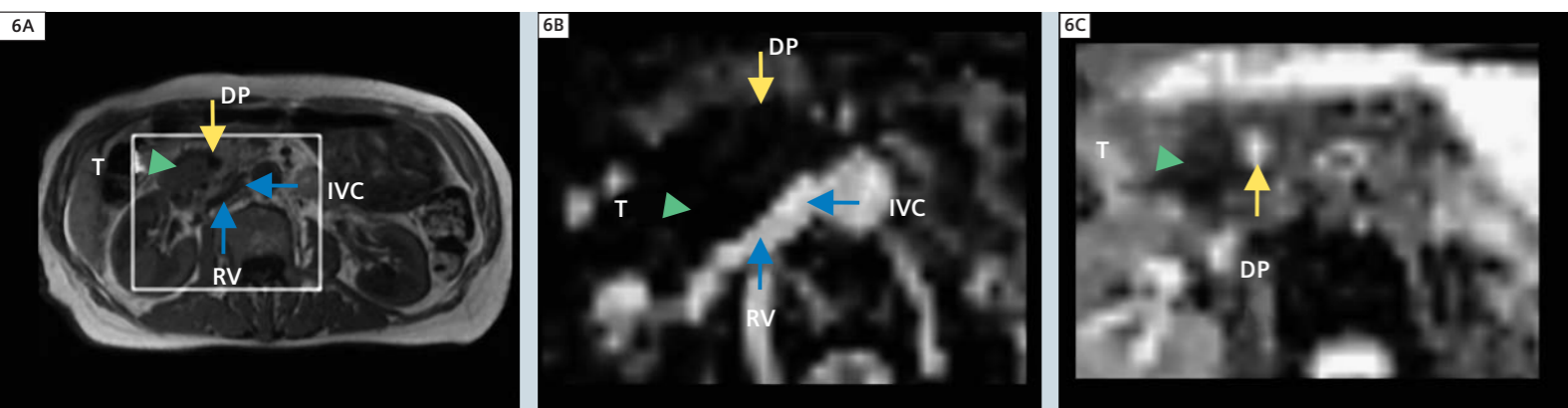
### Pancreatic adenocarcinoma

Four cases of histopathologically confirmed adenocarcinoma are shown in figures 2 through 6.

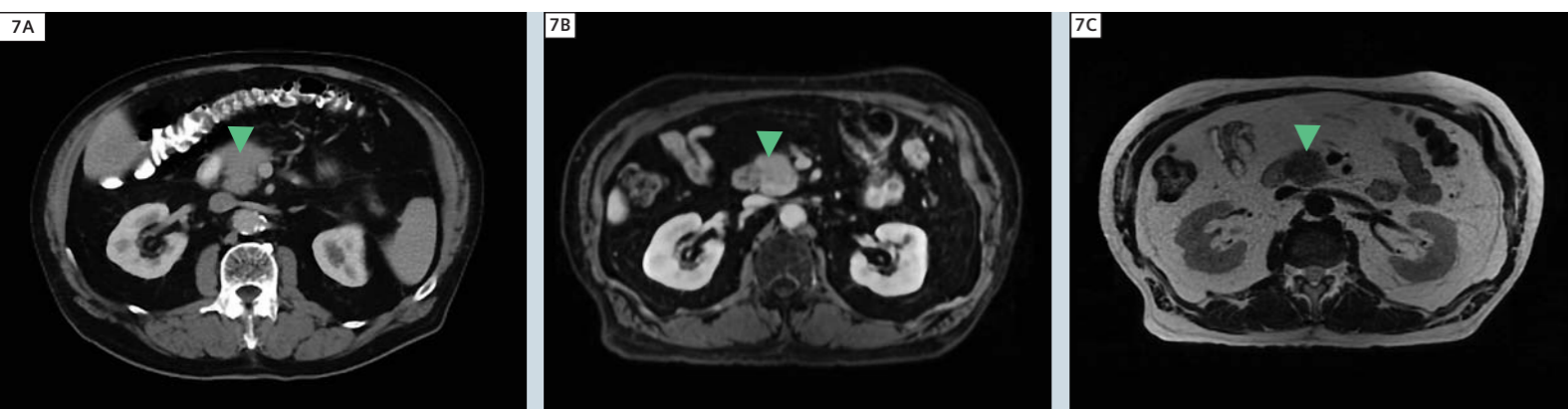
Figure 2 shows a venous phase contrast CT, venous phase contrast T1w and T2w MRI for the first carcinoma case in which a lesion in the head of the pancreas is hypodense in CT and hypointense in both T1w and T2w MRI. Also note the dilated pancreatic duct (DP). The ADC, and *f*-map for this case, presented in figure 3, clearly show the lesion as an area of low apparent diffusion on the ADC and hypo-perfusion (hypointense)

on the *f*-map. Compared to the healthy volunteer, note the extensive area of hypointensity in both the *f*-map and the ADC in the tumor region. Also note that the tumor stands out most prominently on the *f*-map. Furthermore, vessels are best delineated and hyperintense on the *f*-map. However, there is no clear demarcation between the tumor and the dilated duct on the *f*-map. This is better seen on the ADC map where the duct is relatively hyperintense when compared to the tumor.

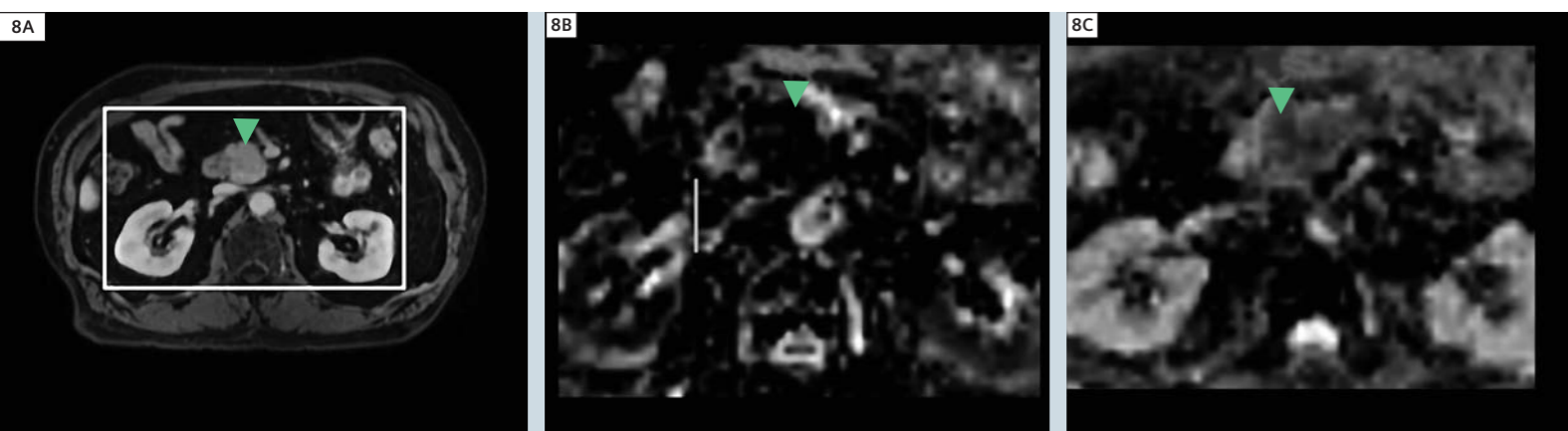
Figure 4 shows a venous phase T1w, ADC and *f*-map for the second carcinoma patient. The lesion again appears as hypointense in T1w, as well as on both the ADC and *f*-map. Again, note the superior depiction of the tumor in the *f*-map where once more the vessels in the vicinity of the tumor are delineated



**6** Patient with a pancreatic cancer in the head of the pancreas. Like in the case presented in figure 3, in the *f*-map (B) the lesion can not be separately distinguished from the adjacent dilated pancreatic duct (DP), whereas the structures can be readily told apart in the ADC-map (C). However, the *f*-map provides much better visualization of the vasculature than the ADC-map, i.e., one can identify the inferior vena cava (IVC), renal vein (RV) and aorta (A). T1w image (A) also provided for comparison. (White rectangle in T1w image = region displayed in other images; T = tumor; IVC = inf. vena cava, RV = renal vein, A = aorta).



**7** Axial venous phase contrast-enhanced CT (A), portal phase contrast-enhanced T1w (B) and T2w (C) images of patient with histopathologically proven chronic pancreatitis in the head of the pancreas (green arrowhead). Note the mass-forming aspect of the lesion, and absence of calcifications in the CT.

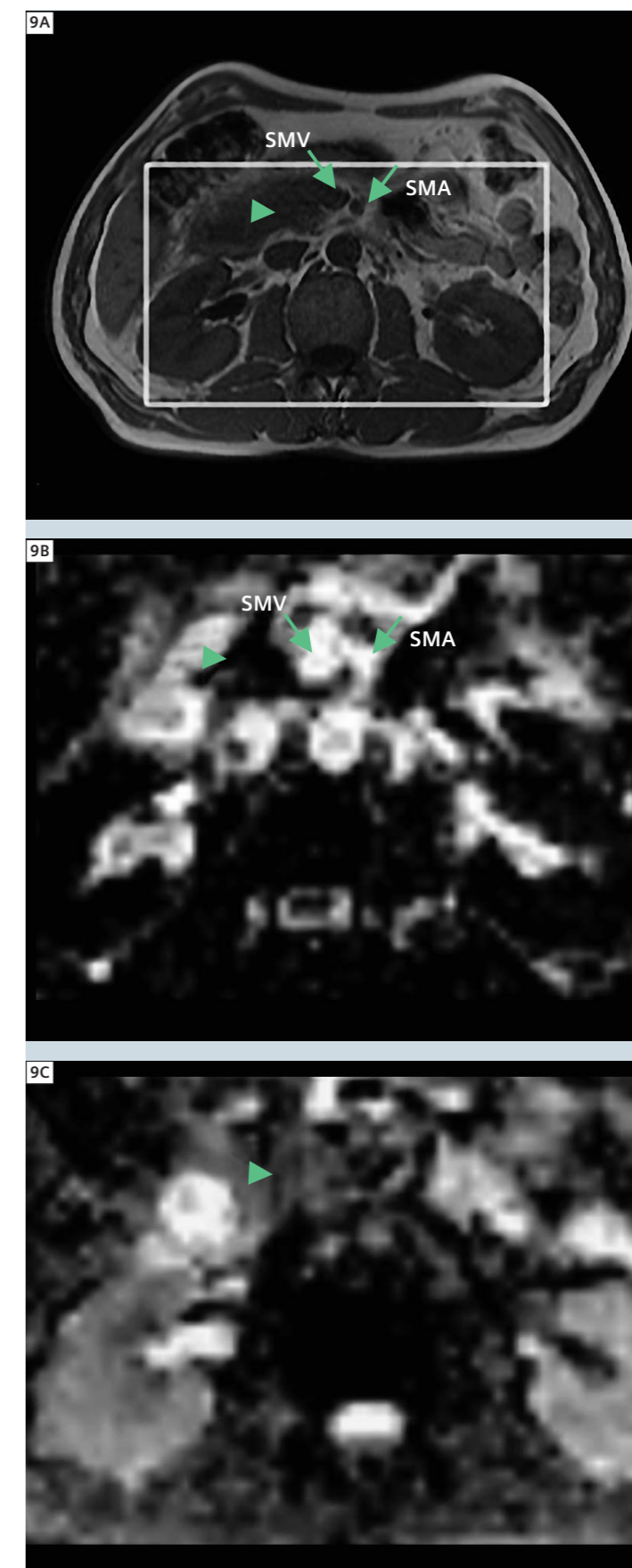


**8** Axial portal phase contrast-enhanced T1w (A), *f*-map (B) and ADC-map (C) of the pancreatitis patient from figure 6. In the contrast-enhanced MRI a slightly hypointense lesion can be seen in the head of the pancreas (large white arrow). It appears markedly hypointense in the *f*-map and only slightly hypointense on the ADC-map (white rectangle in T1w image = region displayed in other images).

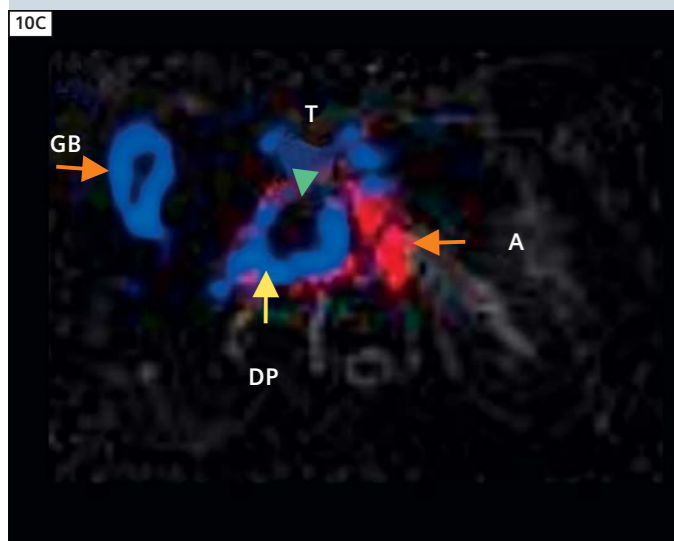
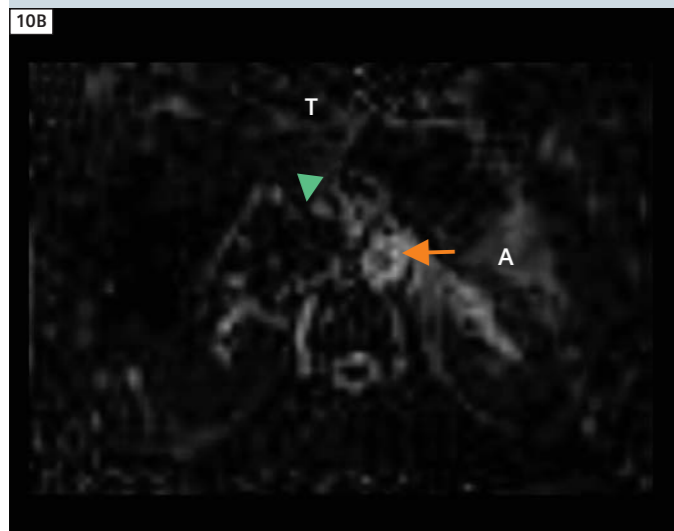
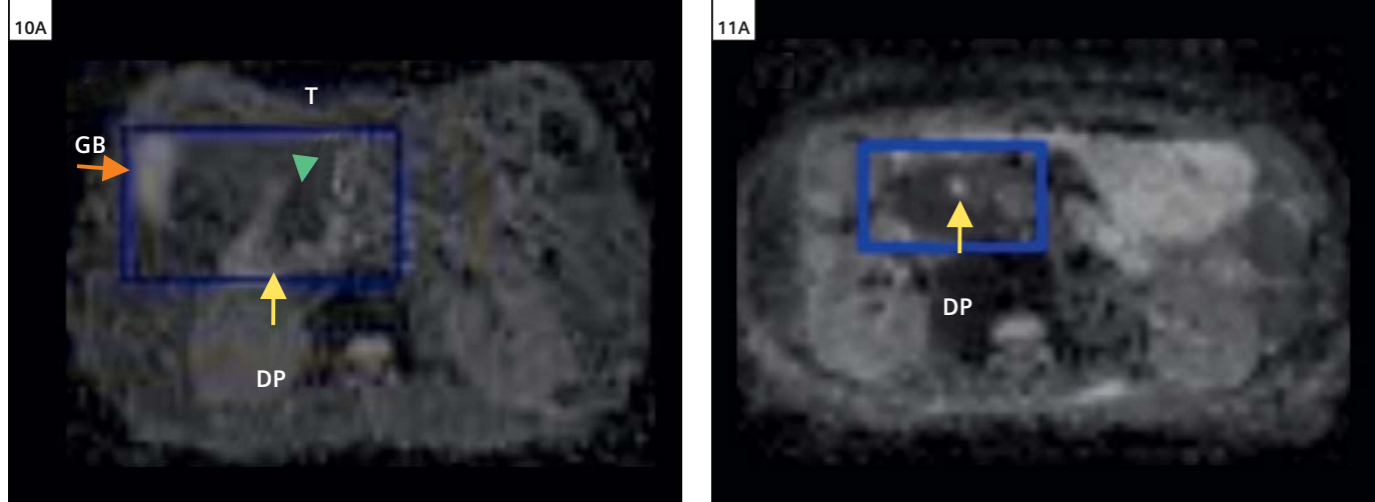
clearly and appear hyperintense. Since no pancreatic duct is present in this slice, the tumor size is depicted accurately in the *f*-map. In the third carcinoma patient (Fig. 5), once more the tumor appears hypointense on the *f*-map. Again, tumor contrast on the *f*-map (5B) is higher than in the ADC-map (5C). In this case, the tumor appears larger than it is on the ADC-map because it is hardly discriminated from the neighboring vessel, whereas the *f*-map, where the vessels are clearly seen as hyperintense, shows the tumor's correct size. Contrary the previous case, the carcinoma in the fourth cancer patient (Fig. 6) is overestimated in the *f*-map when compared to the ADC-map because it lies close to the dilated duct, and both are hypointense. In the ADC-map, the duct appears hyperintense and is thus more readily distinguishable from the lesion as previously seen in patient two (Fig. 4).

**Chronic pancreatitis**

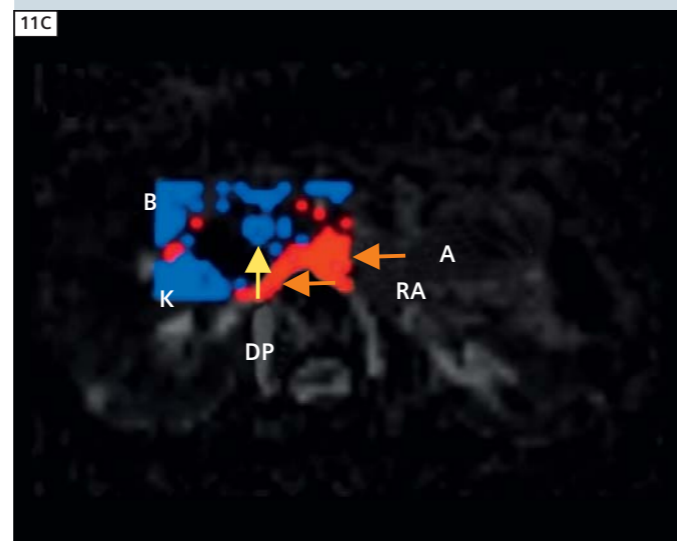
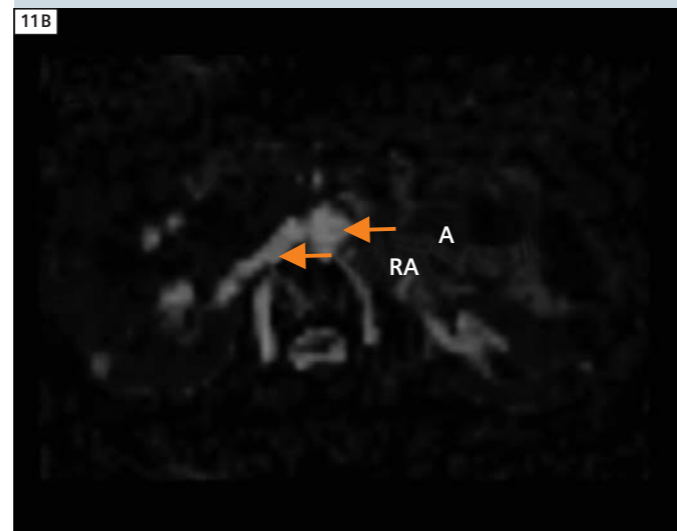
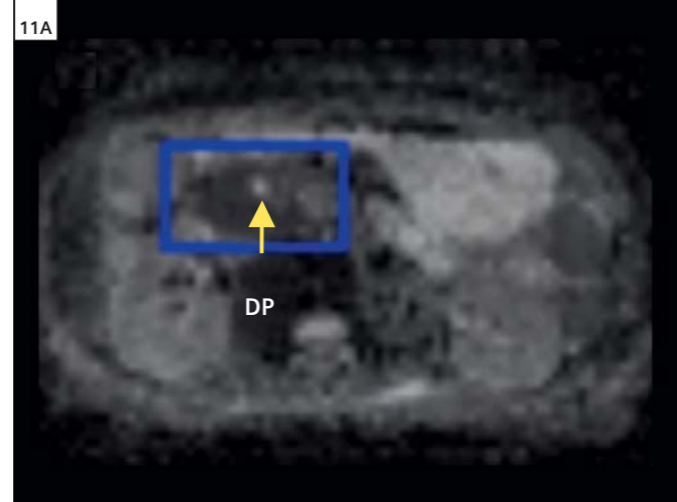
Two cases of histopathologically confirmed pancreatitis mass lesions are shown in figures 7 through 9. Figure 7 shows the venous phase contrast-enhanced CT, portal phase contrast-enhanced T1w, and T2w for the first pancreatitis patient. Note the mass-forming aspect of the lesion. On the ADC and *f*-maps for the same case (Fig. 8), the pancreatitis lesion can be outlined as clearly hypointense in the *f*-map. In the ADC-map, the lesion is partly hypo- and partly isointense compared to the surrounding tissue, and therefore hard to delineate. Note again that the poor lesion/vessel contrast might cause an overestimation of the total lesion size in the ADC-map (e.g. figure 5). Figure 9 shows similar venous phase T1w, ADC, and *f*-maps where the mass-forming pancreatitis is hypodense in the CT and hypointense in T1w/T2w images. Compared to the previous case, note that the lesion is hard to detect on both the conventional MRI and the ADC-map, but that it stands out in stark contrast against both the non-affected pancreatic parenchyma and the surrounding vessels in the *f*-map.



**9** Axial T1w (A), *f*-map (B) and ADC-map (C) for a second patient with histopathologically proven chronic pancreatitis with mass-formation in the head of the pancreas (green arrowhead). The lesion is seen as a well-delineated, hypointense area in the *f*-map, while it is less clearly delineated in the ADC-map. Also well-delineated in the *f*-map as in the T1w image, are the superior mesenteric vein (SMV) and superior mesenteric artery (SMA) (green arrows). (SMA = superior mesenteric artery; SMV = superior mesenteric vein).



**10** Axial ADC-map (A) and  $f$ -map (B) of the pancreatic carcinoma case previously presented in figures 2 and 3 along with an image which integrates both ADC- and  $f$ -map data (C). In the integrated image (C), a color mask is used to segment vascular (red) and ductal (blue) voxels according to  $f$  and ADC ranges described in the text. Note that the tumor is best delineated in the  $f$ -map if the pancreatic duct, which due to its curved path almost completely surrounds the tumor, is color-tagged according to the integrated data. (Dark blue rectangle in ADC-map = region of interest for calculating the color overlay; T = tumor; GB = gall bladder; DP = ductus pancreaticus; A = aorta).



**11** Patient previously presented in figure 6 with the ADC (A) and  $f$ -map (B). Image (C) shows the  $f$ -map with a vascular (red) and ductal (blue) segmentation overlay calculated by integrating the ADC and  $f$  data. Note that the pancreatic duct inside the tumor region can be readily identified on the  $f$ -map only with the help of the overlay. (Dark blue rectangle in ADC-map = region of interest for calculating color overlay; T = tumor; GB = gall bladder; DP = ductus pancreaticus; A = aorta; K = kidney; B = bowel).

### $f$ -maps with an ADC overlay

As seen in the previous cases, the  $f$ -map is superior to the ADC-map considering tumor detection in general. Also, the  $f$ -maps show an increased tumor/vessel contrast when compared to the ADC-maps, but have the disadvantage that adjacent ductal structures may coalesce with the tumor. To circumvent this, we developed a method to integrate both  $f$  and ADC in single parameter images where based on their unique combination of ranges of  $f$  and ADC values, voxels were tagged as belonging to either vessels, ducts, or solid tissue.

In figure 10, the  $f$  and ADC-maps of the patient previously presented in figures 1 and 2 are presented once more (10A, B). Figure 10C shows a color overlay on the  $f$ -map where the pancreatic duct, the gall bladder and the bile ducts are marked blue and the vessels are marked red, defined by the previously described  $f$  and ADC ranges. Note that the tumor size can now be estimated correctly. Figure 11 shows the patient previously presented in figure 6 with the ADC and  $f$ -map (11A, B). Note that the duct inside the tumor region can be readily identified on the  $f$ -map when the color tags are used. Other areas also marked blue include the kidney and the bowel.

### Conclusion

In the cases presented, IVIM-based  $f$ -maps calculated from multiple b-value-weighted magnetic resonance data enabled the delineation of pancreatic lesions and demonstrated advantages over ADC imaging in their ability to distinguish vessels from low-perfused lesions, a crucial element of pancreatic cancer staging. However, which is less apt for distinguishing between lesion and pancreatic or bile ducts as were the ADC-maps. By considering both ADC and  $f$ -maps in combination, better lesion delineation can be achieved than by considering either parameter separately. Concerning lesion pathology differentiation: based on the current experience, it does not seem possible to differentiate between pancreatic carcinoma and pancreatitis using only the imaging aspects of the lesion in the  $f$ -map. Further research

should elucidate the potential of quantitative approaches as means to address this issue. An advantage of ADC and  $f$ -maps when compared to the current imaging standards of conventional CT and ceMRI, is that neither technique uses ionizing radiation nor contrast agent. Since the acquisition takes only approximately 10 minutes, they may be not only safer but also more cost-effective than CT or conventional MRI. Combined ADC/ $f$ -maps may be particularly well suited for the assessment of lesions in patients who can not tolerate contrast agents. In these cases, appropriately combined non-contrast agent T1w/T2w MRI, ADC and  $f$ -maps would be recommended. This combination of non-invasive, non-contrast agent techniques, also shows promise as a screening method for post-treatment follow-up.

\*WIP - Work in progress. This information about this product is preliminary. The product is under development and not commercially available in the U.S., and its future availability cannot be ensured.

### References

- Gemmel C, Eickhoff A, Helmstadter L, et al. Pancreatic cancer screening: state of the art. *Expert Rev Gastroenterol Hepatol* 2009;3:89–96.
- Tamm EP, Silverman PM, Charnsangavej C, et al. Diagnosis, staging, and surveillance of pancreatic cancer. *AJR Am J Roentgenol* 2003;180:1311–1323.
- Tamm EP, Bhosale PR, Lee JH. Pancreatic Ductal Adenocarcinoma: Ultrasound, Computed Tomography, and Magnetic Resonance Imaging Features. *Semin Ultrasound CT MRI* 2007;28:330–338.
- Colagrande S, Carbone SF, Carusi LM, Cova M, Villari N. Magnetic resonance diffusion-weighted imaging: extraneurological applications. *Radiol med* (2006) 111:392–419.
- Koh DM, Collins DJ Diffusion-weighted MRI in the body: applications and challenges in oncology. *AJR Am J Roentgenol* 2007;188:1622–1635.
- Yoshikawa T, Kawamitsu H, Mitchell D, Ohno Y, Ku Y, Seo Y, Fujii M, Sugimura K. ADC Measurement of Abdominal Organs and Lesions Using Parallel Imaging Technique. *AJR* 2006;187:1521–1530.
- Czako L. Diagnosis of early-stage chronic pancreatitis by secretin-enhanced magnetic resonance cholangiopancreatography. *J Gastroenterol* 2007; 42[Suppl XVII]:113–117.
- Balci NC, Momtahan AJ, Akduman EI, Alkaade S, Bilgin M, Burton FR. Diffusion-weighted MRI of the pancreas: correlation with secretin endoscopic pancreatic function test (ePFT). *Acad Radiol*. 2008 Oct;15(10):1264–8.
- Inan N, Arslan A, Akansel G, Anik Y, Demirci A. Diffusion-weighted imaging in the differential diagnosis of cystic lesions of the pancreas. *AJR Am J Roentgenol*. 2008 Oct;191(4):1115–21.
- Fattahi R, Balci NC, Perman WH, Hsueh EC, Alkaade S, Havlioglu N, Burton FR. Pancreatic diffusion-weighted imaging (DWI): comparison between mass-forming focal pancreatitis (FP), pancreatic cancer (PC), and normal pancreas. *J Magn Reson Imaging*. 2009 Feb;29(2):350–6.
- Matsuki M, Inada Y, Nakai G, et al. Diffusion-weighted MR imaging of pancreatic carcinoma. *Abdom Imaging* 2007;32:481–483.
- Muraoka N, Uematsu H, Kimura H, et al. Apparent diffusion coefficient in pancreatic cancer: characterization and histopathological correlations. *J Magn Reson Imaging* 2008;27:1302–1308.
- Le Bihan D. Intravoxel incoherent motion perfusion MR imaging: a wake-up call. *Radiology*. 2008 Dec; 249(3): 748–52.
- Lee SS, Byun JH, Park BJ, Park SH, Kim N, Park B, Kim JK, Lee MG. Quantitative analysis of diffusion-weighted magnetic resonance imaging of the pancreas: usefulness in characterizing solid pancreatic masses. *J Magn Reson Imaging* 2008;28:928–936.
- Luciani A, Vignaud A, Cavet M, Nhieu JT, Mallat A, Ruel L, Laurent A, Deux JF, Brugieres P, Rahmouni A. Liver cirrhosis: intravoxel incoherent motion MR imaging-pilot study. *Radiology*. 2008 Dec;249(3):748–52.
- Le Bihan D MR imaging of incoherent motions: application to diffusion and perfusion in neurologic disorders. *Radiology* 1986;161:401–407.
- Le Bihan D Separation of Diffusion and Perfusion in Intra Voxel Incoherent Motion MR Imaging. *Radiology* 1988;168:497–505.
- Lemke A, Schad LR, Laun F, Stieltjes B. Differentiation of pancreas carcinoma from healthy pancreatic tissue using a wide range of b-values: Comparison of ADC and IVIM parameters. *Proc. Intl. Soc. Mag. Reson. Med.* 17 (2009):666.
- M. Klaus, A. Lemke, K. Grünberg, M. N. Wente, H-U. Kauczor, S. Delorme, L. Grenacher, and B. Stieltjes. Evaluation of low and high b-values for the differentiation between pancreatic carcinoma and chronic pancreatitis using Diffusion-Weighted Imaging. *Proc. Intl. Soc. Mag. Reson. Med.* 17 (2009): 4031.

### Contact

Bram Stieltjes, M.D.  
German Cancer Research Center (DKFZ)  
Department of Radiology - E 010  
Im Neuenheimer Feld 280  
69120 Heidelberg  
Germany  
Tel.: +49(0)6221 42-2492  
b.stieltjes@dkfz.de